

# NUMERICAL SIMULATIONS OF MAGNETOACOUSTIC WAVES IN THE GRAVITATIONALLY STRATIFIED SOLAR ATMOSPHERE

D. DANILKO<sup>a,b</sup>, K. MURAWSKI<sup>b</sup>, R. ERDÉLYI<sup>c</sup>

<sup>a</sup>Group of Astrophysics and Gravity Theory, Institute of Physics  
Maria Curie-Skłodowska University  
Radziszewskiego 10, 20-031 Lublin, Poland

<sup>b</sup>Plasma Accelerators Group  
Institute of Plasma Physics and Laser Microfusion  
Hery 23, 01-497 Warszawa, Poland

<sup>c</sup>Solar Physics and Space Plasma Research Centre  
School of Mathematics and Statistics, University of Sheffield  
The Hicks Building, Hounsfield Road, Sheffield S3 7RH, UK

*(Received January 19, 2012)*

We study impulsively-generated magnetoacoustic waves in the gravitationally stratified solar atmosphere which is permeated by a straight magnetic field. Our numerical model solves two-dimensional magnetohydrodynamic equations in the limit of an ideal plasma and for a temperature profile modelled by a smoothed step function. The results of our simulations agree with the theoretical application of Klein–Gordon equation to fast magnetoacoustic waves propagating in the solar atmosphere. The abovementioned equation introduces a cutoff frequency in the system. Therefore, as the first wave passes, the medium behind it starts to oscillate with a given frequency. Even a small amplitude perturbation in the photosphere generates shock waves in the corona. In addition to that, large impulses (larger than  $\sim 10 \text{ km s}^{-1}$ ) cause oscillations of the plasma in the transition region.

DOI:10.5506/APhysPolB.43.1365

PACS numbers: 52.35.Bj, 96.60.Mz, 96.60.Na, 96.60.P–

## 1. Introduction

Observations of wave phenomena in the solar corona intensified in the past decade. Detailed observational data collected by SOHO, TRACE, Hinode and STEREO satellites provided a stimulus to theoretical studies [1, 2, 3, 4]. Most of these studies are based on magnetohydrodynamic

(MHD) equations which in the solar corona context describe a magnetised medium. The effect of gravity in the solar corona is less important than in the underlying layers of the solar atmosphere. In the case of one-dimensional wave propagation along the gravity, this effect may be accounted for by the Klein–Gordon type of equation. This equation introduces a cutoff frequency below which waves do not propagate [5]. An impulsive perturbation that is governed by the Klein–Gordon equation will result in the presence of a wavefront that is followed by an oscillating wake (*e.g.* [6,7]).

The propagation of acoustic waves in the solar atmosphere, triggered by a photospheric periodic driver was studied by Erdélyi *et al.* [8]. Recent studies of impulsively generated acoustic waves in the solar atmosphere confirmed the significance of the Klein–Gordon equation and extended the theory to non-linear waves and 2D geometry [9]. Our goal here is to generalise these studies to a magnetised plasma. We limit our discussion to impulsively generated magnetoacoustic waves and consider the simplest but representative topology of a straight magnetic field. We will highlight several important issues concerning magnetoacoustic waves triggered by a velocity pulse launched below the transition region.

This paper is organised as follows. The numerical model is described in Sec. 2. The Klein–Gordon equation governing wave propagation is derived in Sec. 3. The numerical results are presented and discussed in Sec. 4. This paper is concluded by a presentation of the main results in Sec. 5.

## 2. A numerical model

### 2.1. Magnetohydrodynamic equations

Our model is based upon the ideal MHD equations:

$$\frac{\partial \varrho}{\partial t} + \nabla \cdot (\varrho \mathbf{V}) = 0, \quad (1)$$

$$\frac{\partial p}{\partial t} + \mathbf{V} \cdot \nabla p = -\gamma p \nabla \cdot \mathbf{V}, \quad (2)$$

$$\varrho \frac{\partial \mathbf{V}}{\partial t} + (\varrho \mathbf{V} \cdot \nabla) \mathbf{V} = -\nabla p + \varrho \mathbf{g} + \frac{1}{\mu} (\nabla \times \mathbf{B}) \times \mathbf{B}, \quad (3)$$

$$\frac{\partial \mathbf{B}}{\partial t} = \nabla \times (\mathbf{V} \times \mathbf{B}), \quad (4)$$

$$= 0, \quad (5)$$

$$p = \frac{k_B}{m} \varrho T. \quad (6)$$

Here  $\varrho$  is mass density,  $\mathbf{V}$  is velocity,  $p$  is kinetic gas pressure,  $\gamma = 5/3$  is adiabatic index,  $\mathbf{g} = [0, 0, -g]$  is gravitational acceleration with  $g = 274 \text{ m s}^{-2}$ ,  $\mathbf{B}$  is magnetic field,  $\mu$  is the magnetic permeability,  $T$  is temperature,  $m$  is mean particle mass and  $k_{\text{B}}$  is Boltzmann's constant.

## 2.2. Equilibrium

We adopt the 1D model of the solar atmosphere in which gravity is balanced by the kinetic pressure gradient force

$$-\varrho_0 g = \frac{\partial p_0}{\partial z}. \quad (7)$$

Henceforth, the subscript 0 corresponds to an equilibrium quantity. The system is assumed to be in a static equilibrium:  $\mathbf{V}_0 = [0, 0, 0]$ , therefore, from Eq. (3) it follows that the magnetic field must be force-free

$$\frac{1}{\mu} (\nabla \times \mathbf{B}_0) \times \mathbf{B}_0 = 0. \quad (8)$$

The above equation is satisfied by a straight magnetic field

$$\mathbf{B}_0 = [B_{0x}, 0, B_{0z}]. \quad (9)$$

From Eq. (7) with the use of Eq. (6) we find

$$p_0(z) = p_{00} \exp \left( - \int_{z_{\text{ref}}}^z \frac{dz'}{\tilde{\Lambda}(z')} \right), \quad (10)$$

and

$$\varrho_0(z) = \frac{p_0(z)}{g \tilde{\Lambda}(z)}. \quad (11)$$

Here

$$\tilde{\Lambda}(z) = \frac{k_{\text{B}} T_0(z)}{mg} \quad (12)$$

is the kinetic pressure scale-height and  $p_{00}$  represents kinetic gas pressure at the reference level  $z_{\text{ref}} = 10 \text{ Mm}$ , corresponding to the top boundary of the simulation region. We can rewrite Eq. (12), using Eq. (6), as

$$\tilde{\Lambda}(z) = \frac{c_{\text{s}}^2(z)}{\gamma g}. \quad (13)$$

Here  $c_s(z)$  is sound speed, defined as follows

$$c_s(z) = \sqrt{\frac{\gamma p_0(z)}{\varrho_0(z)}}. \quad (14)$$

The plasma  $\beta$  parameter is defined as the ratio of kinetic gas pressure to magnetic pressure

$$\beta = \frac{p_0(z)}{B_0^2/2\mu}. \quad (15)$$

In the solar corona  $\beta \ll 1$  and therefore, we would refer to it as a low- $\beta$  medium. The profile of  $\beta$  and sound speed  $c_s(z)$  is shown in Fig. 1. We assume that the equilibrium temperature profile is given as [10, 11]

$$T_0(z) = \frac{1}{2}(T_c + T_{\text{ph}}) + \frac{1}{2}(T_c - T_{\text{ph}}) \tanh\left(\frac{z - z_{\text{tr}}}{z_w}\right), \quad (16)$$

where  $T_{\text{ph}} = 5000$  K denotes the temperature of plasma at  $z = 0$  (bottom of the simulation region), which corresponds to a region located 500 km above the optical surface of the photosphere, just above the photospheric temperature minimum;  $T_c = 10^6$  K is the temperature of the solar corona;  $z_{\text{tr}} = 1.5$  Mm is the location of transition region and  $z_w = 0.2$  Mm is its width. The temperature and mass density profiles are shown in Fig. 2.

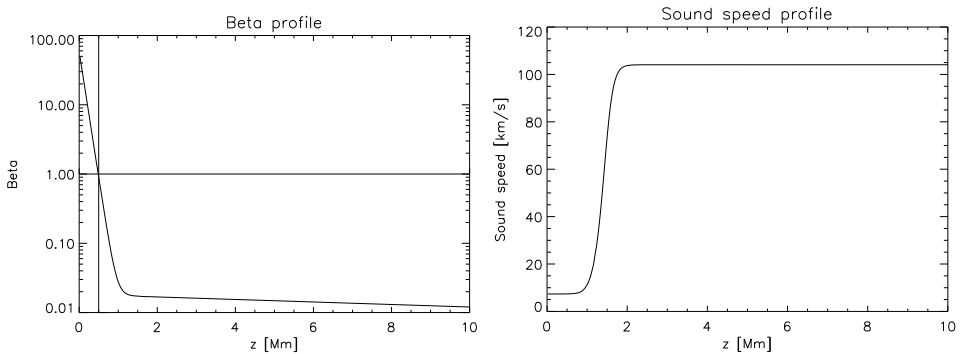


Fig. 1. Spatial profiles of plasma  $\beta$  (left) and sound speed (right).

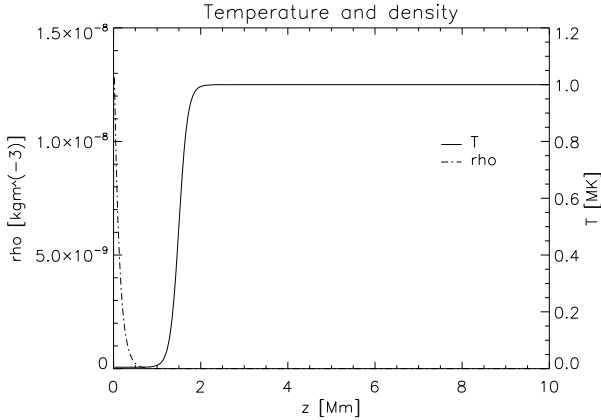


Fig. 2. Spatial profiles of temperature and mass density.

### 3. Klein–Gordon equation

It has been shown by Roberts [12] (following Lamb [5]) that, in the absence of magnetic field, sound waves propagating along the gravity action in a gravitationally stratified atmosphere are described by the Klein–Gordon equation

$$\frac{\partial^2 Q}{\partial t^2} - c_s^2(z) \frac{\partial^2 Q}{\partial z^2} + \Omega_s^2(z) Q = 0, \quad (17)$$

where  $Q = Q(z, t)$  is a normalised function of velocity and  $\Omega_s(z)$  is the local critical frequency

$$\Omega_s^2(z) = \frac{c_s^2(z)}{4\tilde{\Lambda}^2(z)} \left[ 1 + 2 \frac{\partial \tilde{\Lambda}(z)}{\partial z} \right]. \quad (18)$$

In the case of an isothermal atmosphere, the kinetic pressure scale-height and the sound speed are constant ( $\tilde{\Lambda}(z) = \tilde{\Lambda}_0$ ,  $c_s(z) = c_s$ ) and  $\Omega_s(z)$  becomes the acoustic cutoff frequency,  $\Omega_{ac}$ , given as

$$\Omega_{ac} = \frac{c_s}{2\tilde{\Lambda}_0}. \quad (19)$$

The corresponding dispersion relation

$$\omega^2 = k_z^2 c_s^2 + \Omega_{ac}^2 \quad (20)$$

shows that only waves with frequencies higher than the acoustic cutoff frequency,  $\omega > \Omega_{ac}$ , propagate through the medium. It has also been shown by Roberts [12] that the medium behind the wavefront creates a wake which oscillates with the acoustic cutoff frequency.

In the following sections, we derive a governing equation (in the form of the Klein–Gordon equation) for a stratified non-isothermal atmosphere with an embedded magnetic field and analyse and compare it with the above results.

### 3.1. The case of a vertical magnetic field

We consider the case of a vertical magnetic field by setting  $B_{0x} = 0$  and  $B_{0z} = B_0$  in Eq. (9). After linearising Eqs. (3) and (4) we find that small amplitude, vertically propagating transverse waves are described by

$$\frac{\partial^2 V_x}{\partial t^2} = c_A^2(z) \frac{\partial^2 V_x}{\partial z^2}. \quad (21)$$

Here

$$c_A(z) = \frac{B_0}{\sqrt{\mu \rho_0(z)}} \quad (22)$$

is the local Alfvén speed.

Equation (21) describes the vertical evolution of both a transverse Alfvén wave [13] and a transverse fast MHD wave. In the considered geometry, the two waves are indistinguishable as each of them travels along the magnetic field at the Alfvén speed  $c_A$ . Since  $\frac{d}{dz} c_A(z) > 0$ , the amplitude of the waves grows with altitude.

Similarly, by linearising Eqs. (2)–(4) and in the limit of low plasma- $\beta$  these equations describe (approximately) slow magnetoacoustic waves

$$\frac{\partial^2 V_z}{\partial t^2} = c_s^2(z) \frac{\partial^2 V_z}{\partial z^2} - \gamma g \frac{\partial V_z}{\partial z}. \quad (23)$$

The above equation was used by Roberts [14] to describe slow magnetoacoustic waves in a low plasma- $\beta$  medium. A more adequate derivation of slow magnetoacoustic equations which are valid for arbitrary plasma- $\beta$  can also be found in Roberts [14]. Equation (23) can be transformed to the Klein–Gordon equation (17) (see [12]), which implies that the local critical frequency of longitudinal MHD waves is given by Eq. (18) and that these waves obey the Klein–Gordon equation in the considered geometry.

### 3.2. The case of a horizontal magnetic field

Let us discuss now the case of horizontal magnetic field by setting  $B_{0x} = B_0$  and  $B_{0z} = 0$  in Eq. (9). Linearisation of Eqs. (2)–(4) yields that small amplitude fast magnetoacoustic waves are described by

$$\frac{\partial^2 V_z}{\partial t^2} = c_f^2 \frac{\partial^2 V_z}{\partial z^2} - \gamma g \frac{\partial V_z}{\partial z}, \quad (24)$$

where

$$c_f = \sqrt{c_s^2 + c_A^2} \quad (25)$$

denotes a fast speed.

Equation (24) indicates that there is no coupling between fast and slow magnetoacoustic waves. By introducing a new variable,  $U$ ,

$$V_z(z, t) = U(z, t) \exp\left(\frac{\gamma g}{2} \int \frac{dz}{c_f^2(z)}\right) \quad (26)$$

we transform Eq. (24) to a Klein–Gordon equation

$$\frac{\partial^2 U}{\partial t^2} - c_f^2(z) \frac{\partial^2 U}{\partial z^2} + \Omega_{fc}^2(z) U = 0, \quad (27)$$

where

$$\Omega_{fc}^2(z) = \frac{\gamma^2 g^2}{4c_f^2(z)} \left[ 1 + 2 \frac{\partial \tilde{\Lambda}_f(z)}{\partial z} \right] \quad (28)$$

is the fast magnetoacoustic cutoff frequency and  $\tilde{\Lambda}_f(z)$  is defined as follows

$$\tilde{\Lambda}_f(z) = \frac{c_f^2(z)}{\gamma g}. \quad (29)$$

It is noteworthy that for the magnetic-free case ( $\mathbf{B} = 0$ ), Eq. (28) transforms to Eq. (18). From MHD equations we infer that slow waves are absent from the system.

## 4. Numerical results

We solve Eqs. (1)–(6) using the Athena code [15]. A modified Force Flux [16] and a second-order Godunov method [17] are used for performing the simulations. We limit ourselves to a two-dimensional problem with the computation box of 10 Mm  $\times$  10 Mm that is resolved by up to 512  $\times$  512 numerical cells.

#### 4.1. Perturbation

The equilibrium profiles of Eqs. (9)–(11) are perturbed by an initial pulse in velocity

$$\delta\mathbf{V}(x, z, t_0) = [\alpha_x \cdot \delta V, 0, \alpha_z \cdot \delta V], \quad (30)$$

where  $\alpha_x, \alpha_z \in \{0, 1\}$  are parameters used to launch a pulse perpendicular to the magnetic field, and

$$\delta V = A_V \exp \left[ -\frac{(x - x_0)^2}{4w_x^2} - \frac{(z - z_0)^2}{4w_z^2} \right]. \quad (31)$$

Here  $A_V$  is the amplitude of the initial pulse that is launched at  $(x_0, z_0)$  and  $w_x, w_z$  are its half-widths. We set and hold fixed  $x_0 = 0$  Mm and  $z_0 = 0.5$  Mm, which means that the perturbation is launched below the transition region. We consider two cases: a wavefront with  $w_x \rightarrow \infty, w_z = 0.25$  Mm and a localised pulse with  $w_x = w_z = 0.25$  Mm.

In the present paper, we study both the horizontal and vertical orientation of the magnetic field by choosing either  $B_{0z} = 0$  or  $B_{0x} = 0$ .

#### 4.2. Vertical magnetic field

Here, we consider the case of a vertically aligned equilibrium magnetic field by setting  $B_{0x} = 0$  in Eq. (9).

##### 4.2.1. A wavefront in horizontal velocity

Let us perturb the equilibrium state of Eqs. (9)–(11) by a wavefront in  $V_x$  of Eq. (30) with  $\alpha_x = 1, \alpha_z = 0$  and  $w_x \rightarrow \infty$ . Such an initial perturbation triggers both fast and slow magnetoacoustic waves as shown in Sec. 3.1. Figure 3 confirms that the results of the simulation agree very well with the predictions based on the analytical equations derived in Sec. 3.1. The fast wave (coupled with the Alfvén wave mode) propagates along the magnetic field lines (Fig. 3 (top left)). The upward propagating wave accelerates due to inhomogeneous Alfvén speed, while the downward propagating pulse decelerates. The former leaves the computational domain through the upper boundary and the latter experiences partial reflection from the dense layers of the chromosphere.

The slow wave also splits into two counter-propagating wavefronts. It was shown in Sec. 3.1 that the behaviour of slow waves is governed by the Klein–Gordon equation, implying that the medium behind the wavefront oscillates with the acoustic cutoff frequency [12]. This is clearly seen in Fig. 3 (top right). Wavefronts that follow, elevate the plasma triggering oscillations of the transition region, as shown in Fig. 3 (bottom).

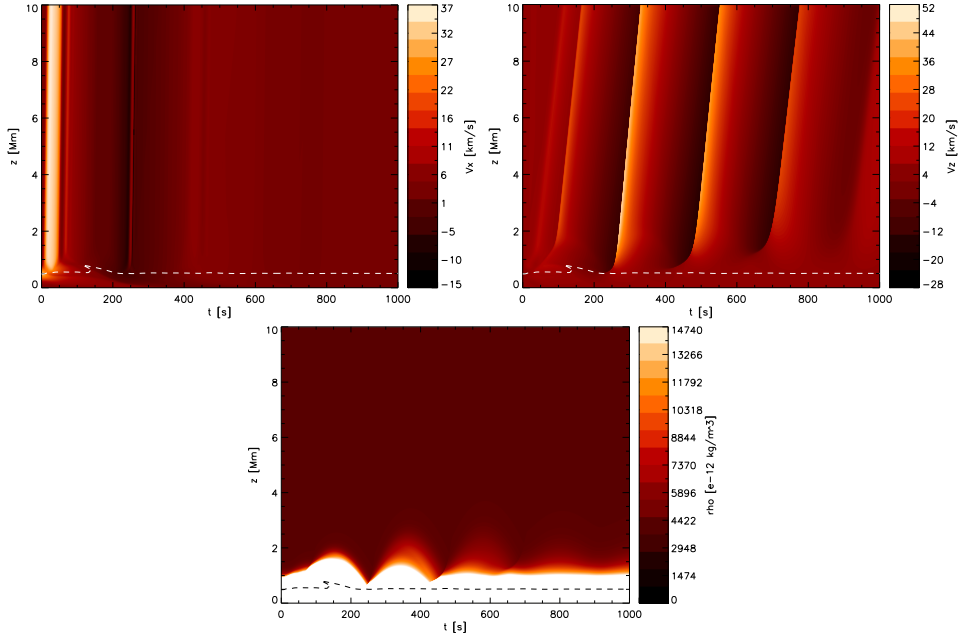


Fig. 3. Time dependence of  $V_x$  (top left),  $V_z$  (top right) and  $\rho$  (bottom) for a wavefront of Eq. (30) with  $\delta V_z = 0$ ,  $z_0 = 0.5$  Mm,  $w_x = w_z = 0.25$  Mm and  $A_V = 30$  km s $^{-1}$  collected at  $x = 0$  Mm. The case of a vertical equilibrium magnetic field with  $B_{ex} = 0$  in Eq. (9). Dashed line represents  $\beta = 1$  level.

Next, we perform a Fast Fourier Transform of the  $V_z$  component of velocity that is collected at the altitude  $z = 5$  Mm. The result is shown in Fig. 4. By analysing the results of a simulation we estimate the main period of oscillations to be:  $P \cong 205$  s.

The considered atmosphere is non-isothermal, which implies that there is a multitude of local critical frequencies. In order to evaluate the global cutoff period, we consider a number of isothermal atmospheres in a temperature range covered by temperatures of the system. From Eq. (19) we compute the acoustic cutoff period for each temperature, recalling that  $P = 2\pi/\Omega$ . Since each elevation of our simulation region has a different temperature, we can plot the obtained cutoff periods against altitude  $z$ , instead of temperature. This gives us a hypothetical cutoff period profile depicted in Fig. 5. The global cutoff period is the smallest value on the above-mentioned plot, which is  $\sim 204$  s. This is in perfect agreement with the value obtained earlier in the simulation.

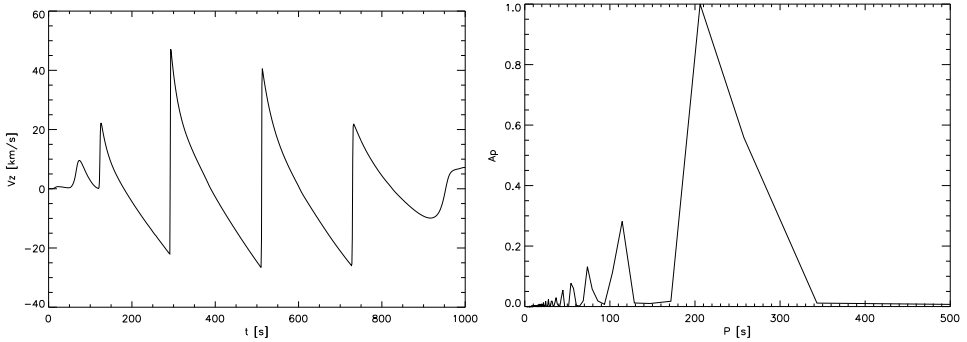


Fig. 4. Time dependence of  $V_z$  (left) collected at  $x = 0$  Mm,  $z = 5$  Mm and a corresponding Fourier power spectrum (right) for a wavefront of Eq. (30) with  $\delta V_z = 0$ ,  $z_0 = 0.5$  Mm,  $w_x = w_z = 0.25$  Mm and  $A_V = 30$  km s $^{-1}$ . The case of a vertical equilibrium magnetic field with  $B_{ex} = 0$  in Eq. (9).

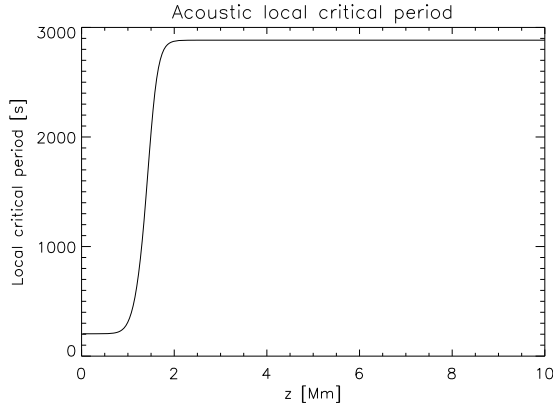


Fig. 5. A hypothetical acoustic cutoff period profile, calculated for isothermal atmospheres from Eq. (19).

#### 4.2.2. A localised pulse in horizontal velocity

Let us now extend the simulations performed in Sec. 4.2.1 to a fully 2D case by perturbing the equilibrium state of Eqs. (9)–(11) by a localised pulse of Eq. (30) with  $\alpha_x = 1$  and  $\alpha_z = 0$ . This perturbation is launched at the same altitude as previously. The impulse in  $V_x$  propagates as a quasi-circular fast wave as shown in Fig. 6. From this figure we also see that in lower regions of the atmosphere, where the plasma  $\beta$  parameter is high, slow waves are triggered. Since the magnetic field is vertical, slow waves propagate along the gravity action as shown in Fig. 6. In Fig. 7, we demonstrate that the medium behind the first wave oscillates as predicted by the Klein–Gordon equation for a 1D case.

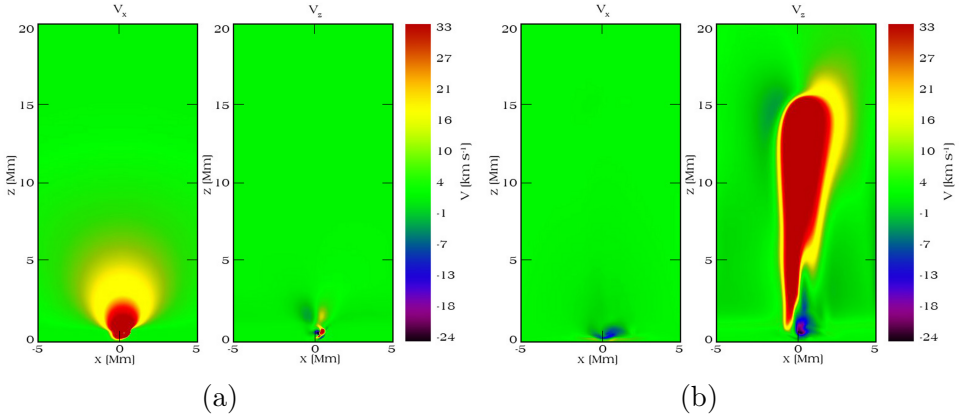


Fig. 6. Spatial plots of  $V_x$  and  $V_z$  for  $t = 15$  s (a) and  $t = 150$  s (b). The case of a vertical equilibrium magnetic field.

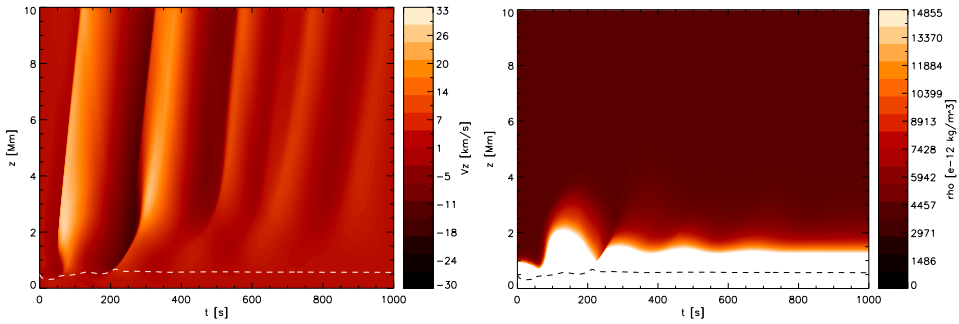


Fig. 7. Time dependence of  $V_z$  (left) and  $\rho$  (right) for the localised pulse of Eq. (30) with  $\delta V_z = 0$ ,  $z_0 = 0.5$  Mm,  $w_x = w_z = 0.25$  Mm and  $A_V = 50$  km s $^{-1}$  collected at  $x = 0$  Mm. The case of a vertical equilibrium magnetic field with  $B_{ex} = 0$  in Eq. (9). Dashed line represents  $\beta = 1$  level.

The result of a Fast Fourier Transform of  $V_z$  component of velocity determined at the altitude  $z = 5$  Mm is shown in Fig. 8. By analysing the plot we estimate the main period of oscillations to be:  $P \cong 210$  s, which is in good agreement with theoretical and numerical results obtained for a 1D scenario.

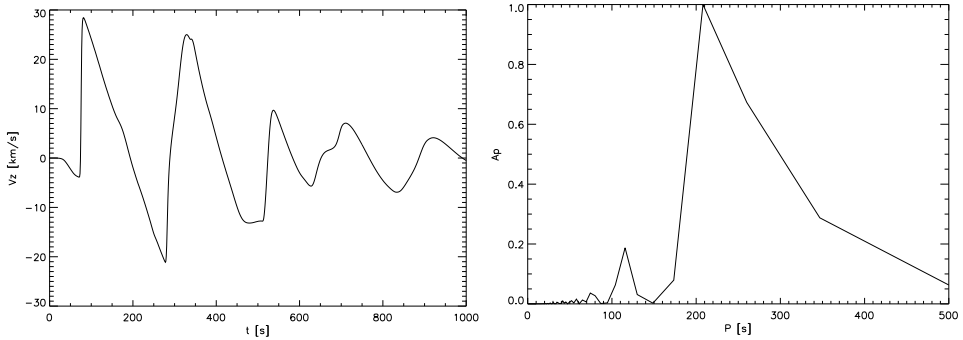


Fig. 8. Time dependence of  $V_z$  (left) collected at  $x = 0$  Mm,  $z = 5$  Mm and a corresponding Fourier power spectrum (right) for the localised pulse of Eq. (30) with  $\delta V_z = 0$ ,  $z_0 = 0.5$  Mm,  $w_x = w_z = 0.25$  Mm and  $A_V = 50$  km s $^{-1}$ . The case of a vertical equilibrium magnetic field with  $B_{ex} = 0$  in Eq. (9).

### 4.3. Horizontal magnetic field

Here, we consider the case of a horizontally aligned equilibrium magnetic field by setting  $B_{0z} = 0$  in Eq. (9).

#### 4.3.1. A wavefront in vertical velocity

We perturb the equilibrium state of Eqs. (9)–(11) by a wavefront of Eq. (30) with  $\alpha_x = 0$ ,  $\alpha_z = 1$  and  $w_x \rightarrow \infty$ . In agreement with Sec. 3.2, in this case only fast waves propagate through the medium, travelling at the fast speed. In Fig. 9, the oscillating wake that formed behind the wavefront is clearly seen, the creation of which was predicted by the Klein–Gordon equation in Sec. 3.2.

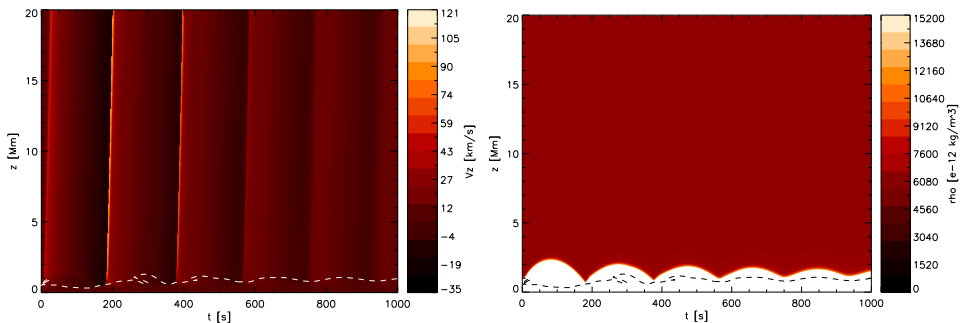


Fig. 9. Time dependence of  $V_z$  (left) and  $\rho$  (right) for the localised initial pulse of Eq. (30) with  $\delta V_x = 0$ ,  $z_0 = 1.0$  Mm,  $w_x = w_z = 0.25$  Mm and  $A_V = 100$  km s $^{-1}$  collected at  $x = 0$  Mm. The case of a horizontal equilibrium magnetic field with  $B_{ez} = 0$  in Eq. (9). Dashed line represents  $\beta = 1$  level.

We then perform FFT of the  $V_z$  component of velocity at the altitude  $z = 5$  Mm and estimate the main period of oscillations to be:  $P \cong 205$  s (based on the results depicted in Fig. 10).

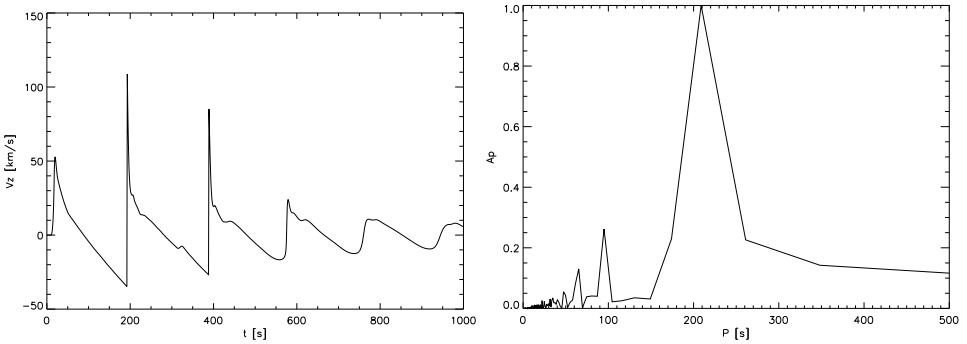


Fig. 10. Time dependence of  $V_z$  (left) collected at  $x = 0$  Mm,  $z = 5$  Mm and a corresponding Fourier power spectrum (right) for a wavefront of Eq. (30) with  $\delta V_x = 0$ ,  $z_0 = 1.0$  Mm,  $w_x = w_z = 0.25$  Mm and  $A_V = 100$  km s $^{-1}$ . The case of a horizontal equilibrium magnetic field with  $B_{ez} = 0$  in Eq. (9).

Figure 11 shows a hypothetical profile of a fast cutoff period, obtained from Eq. (28) in a similar manner as explained in Sec. 4.2.1. The lowest value of a fast cutoff period is  $\sim 206$  s, which agrees with the value obtained in the simulation.

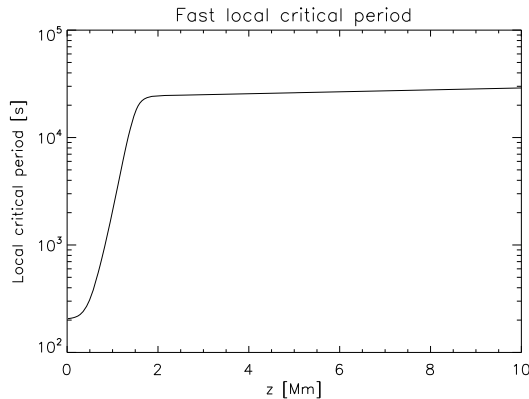


Fig. 11. A hypothetical fast cutoff period profile, calculated for isothermal atmospheres from Eq. (28).

### 4.3.2. A localised pulse in vertical velocity

Finally, let us perturb the equilibrium state of Eqs. (9)–(11) by a localised pulse of Eq. (30) with  $\alpha_x = 0$  and  $\alpha_z = 1$ . As in previous sections, we launch this perturbation within the transition region:  $z_0 < z_{\text{tr}} = 1.5$  Mm.

The results of the simulation are presented in Fig. 12. One can see that the difference between a 2D case and a 1D scenario of Fig. 9 is significant. The period of oscillations is significantly shorter and the amplitude is strongly attenuated (Fig. 13).

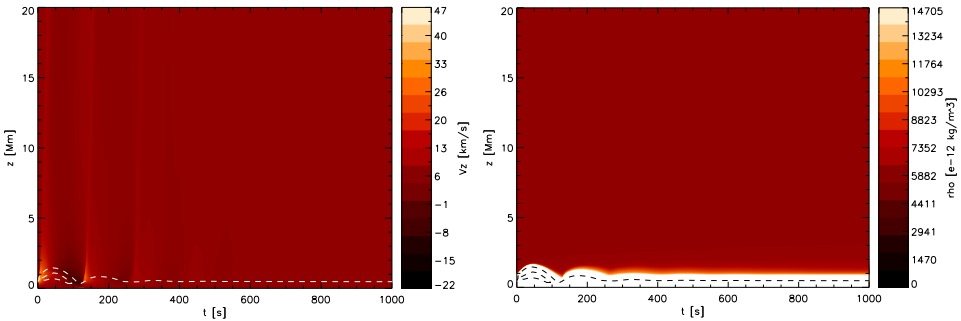


Fig. 12. Time dependence of  $V_z$  (left) and  $\rho$  (right) for the localised initial pulse of Eq. (30) with  $\delta V_x = 0$ ,  $z_0 = 1.0$  Mm,  $w_x = w_z = 0.25$  Mm and  $A_V = 50$  km s $^{-1}$  collected at  $x = 0$  Mm. The case of a horizontal equilibrium magnetic field with  $B_{ez} = 0$  in Eq. (9).

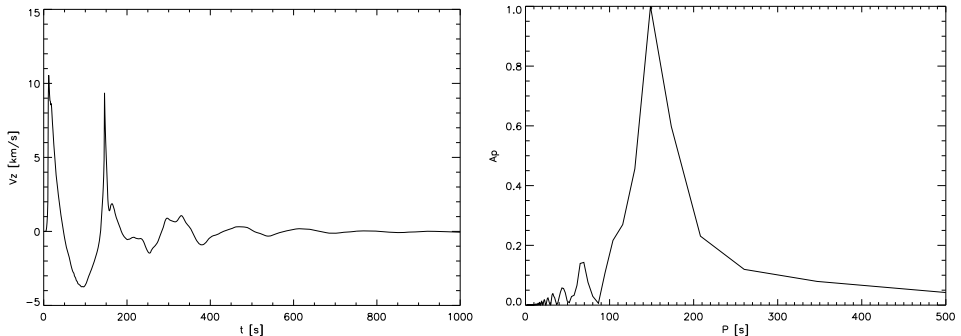


Fig. 13. Time dependence of  $V_z$  (left) collected at  $x = 0$  Mm,  $z = 5$  Mm and a corresponding Fourier power spectrum (right) for the localised initial pulse of Eq. (30) with  $\delta V_x = 0$ ,  $z_0 = 1.0$  Mm,  $w_x = w_z = 0.25$  Mm and  $A_V = 50$  km s $^{-1}$ . The case of a horizontal equilibrium magnetic field with  $B_{ez} = 0$  in Eq. (9).

FFT of the  $V_z$  component of velocity at  $z = 5$  Mm is performed and the results (shown in Fig. 13) yield that the main period of oscillations is:  $P \cong 150$  s, which is much lower than the value obtained in a 1D simulation. In order to explain this apparent inconsistency, we plot time variance of the cutoff period, estimated from Eq. (19) as the lowest value of the local critical period. In Fig. 14, we show that the cutoff period changes from  $P \cong 165$  s to  $P \cong 240$  s, which may explain the difference between the theoretical and the numerical cutoff period.

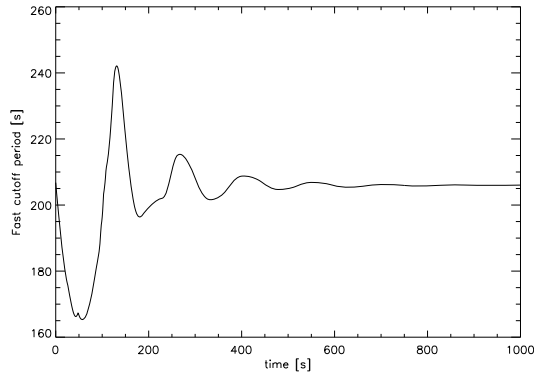


Fig. 14. Time dependence of  $\min(P_f)$  calculated from Eq. (19) for the localised initial pulse of Eq. (30) with  $\delta V_x = 0$ ,  $z_0 = 1.0$  Mm,  $w_x = w_z = 0.25$  Mm and  $A_V = 50$  km s $^{-1}$ . The case of a horizontal equilibrium magnetic field with  $B_{ez} = 0$  in Eq. (9).

## 5. Summary and discussion

In this paper, we have studied impulsively generated magnetoacoustic waves in the middle layers of the solar atmosphere. A constant gravity and a straight magnetic field topology were taken into consideration in order to capture the essential physics and to be able to obtain analytical formula for the propagation of magnetoacoustic waves. The temperature profile of the solar atmosphere above the photospheric minimum was approximated with a model also used by Cargill *et al.* [10] and Del Zanna *et al.* [11].

Our results can be summarised as follows. An impulsive perturbation triggers magnetoacoustic waves which propagate along the gravity action as described by the Klein–Gordon type of equation. A trailing wake oscillates with a cutoff frequency, creating waves with a given period. Both the acoustic cutoff period and the fast cutoff period were in the range  $P_f \cong P \sim 200$ –210 s.

The initial pulse launched below the transition region moves the dense layers upwards triggering oscillations. The vertical motion of the chromospheric gas caused by Alfvén or acoustic-gravity waves was associated, *e.g.* by Hollweg [18], with the generation of spicules. In the case of magnetoacoustic waves, the pulse results in oscillations of the transition region as can be seen in Figs. 3, 7, 9 and 12 (right). The characteristics of these oscillations (period, amplitude) does not match the characteristics of a spicule [19], but remain in the same range, which creates opportunity for future studies. Similar oscillations of the transition region, triggered by a pair of periodic drivers, were found to result in surface waves [20].

Oscillations of the transition region result in mass density profile modification. The extent of these deviations from the equilibrium state depends on the amplitude of the initial perturbation. The change of mass density profile alters the cutoff frequency in Eq. (27), which in linear approximation depends only on the initial configuration. This is the reason why numerical simulations revealed different cutoff periods for the same equilibrium profiles, which was especially prominent in the case presented in Sec. 4.3.2. In order to investigate this problem in a greater detail, a more realistic model should be incorporated.

Roberts and Webb [21] obtained similar results for a vertical flux tube to those presented in Sec. 4.2. They calculated an acoustic cutoff period to be  $P = 199$  s at  $z = 0$  Mm (corresponding to a level located 500 km above the optical surface of the Sun) and  $P = 200$  s at  $z = 500$  Mm. These numbers are in a very good agreement with the results presented in this paper. However, the minimal value of the cutoff period obtained by Roberts and Webb [21] was  $P = 159$  s at  $z = 100$  Mm, which differs from the profile of the acoustic cutoff period depicted in Fig. 5. This difference stems from using an alternative profile of the solar atmosphere.

Further studies of magnetoacoustic waves should be undertaken in order to understand their influence on various solar phenomena in a greater detail. The studies presented in this paper can be extended to examine the importance of magnetoacoustic waves in excitation and attenuation of oscillations in coronal loops, the generation of spicules [22] and even the heating of the corona.

D. Daniłko acknowledges MSRC of the School of Mathematics and Statistics, Sheffield, UK for supporting his visit to the University of Sheffield. R. Erdélyi acknowledges M. Kéray for patient encouragement and is grateful to NSF, Hungary (OTKA, Ref. No. K83133).

REFERENCES

- [1] V.M. Nakariakov, E. Verwichte, *Living Rev. Solar Phys.* **2**, 3 (2005).
- [2] D. Banerjee, R. Erdélyi, R. Oliver, E. O'Shea, *Sol. Phys.* **246**, 3 (2007).
- [3] M.J. Aschwanden, in: *Waves and Oscillations in the Solar Atmosphere: Heating and Magneto-Seismology*, Proc. IAU Symp. 247, ed. R. Erdélyi, C.A. Mendoza-Briceño, Cambridge University Press, Cambridge 2008, p. 257.
- [4] T. Wang, *Space Sci. Rev.* **158**, 397 (2011).
- [5] H. Lamb, *Proc. London Math. Soc.* **7**, 122 (1909).
- [6] I.C. Rae, B. Roberts, *Astrophys. J.* **256**, 761 (1982).
- [7] S.P. James, R. Erdélyi, B. De Pontieu, *Astron. Astrophys.* **406**, 715 (2003).
- [8] R. Erdélyi, C. Malins, G. Tóth, B. De Pontieu, *Astron. Astrophys.* **467**, 1299 (2007).
- [9] M. Gruszecki *et al.*, *Acta Phys. Pol. B* **42**, 1333 (2011).
- [10] P.J. Cargill, D.S. Spicer, S.T. Zalesak, *Astrophys. J.* **488**, 854 (1997).
- [11] L. Del Zanna, E. Schaekens, M. Velli, *Astron. Astrophys.* **431**, 1095 (2005).
- [12] B. Roberts, in: Proc. SOHO 13 *Waves, Oscillations and Small-Scale Transient Events in the Solar Atmosphere: A Joint View from SOHO and TRACE*, ed. R. Erdélyi, J.L. Ballester, B. Fleck, ESA SP-547, 1, 2004.
- [13] K. Murawski, Z.E. Musielak, *Astron. Astrophys.* **518**, A37 (2010).
- [14] B. Roberts, *Phil. Trans. R. Soc.* **A364**, 447 (2006).
- [15] J.M. Stone, M.N. Lemaster, *Rev. Mex. Astron. Astrofis. (SC)* **36**, 31 (2009).
- [16] E. Toro, *Riemann Solvers and Numerical Methods for Fluid Dynamics*, Springer, 1999.
- [17] P. Collela, P.R. Woodward, *J. Comp. Phys.* **54**, 174 (1984).
- [18] J.V. Hollweg, *Astrophys. J.* **257**, 345 (1982).
- [19] B. De Pontieu, R. Erdélyi, S.P. James, *Nature* **430**, 536 (2004).
- [20] C. Malins, R. Erdélyi, *Sol. Phys.* **246**, 41 (2007).
- [21] B. Roberts, A.R. Webb, *Sol. Phys.* **56**, 5 (1978).
- [22] K. Murawski, T. Zaqarashvili, *Astron. Astrophys.* **519**, A8 (2010).